# CRACK INITIATION IN SMOOTH FATIGUE SPECIMENS OF AUSTENITIC STAINLESS STEEL IN LIGHT WATER REACTOR ENVIRONMENTS

**Jean L. Smith**
Materials Science and Engineering Department
Rensselaer Polytechnic Institute
Troy, New York 12180

**Omesh K. Chopra**
Energy Technology Division
Argonne National Laboratory
Argonne, Illinois 60439



## ABSTRACT

The fatigue design curves for structural materials specified in Section III of the ASME Boiler and Pressure Vessel Code are based on tests of smooth polished specimens at room temperature in air. The effects of light water reactor (LWR) coolant environments are not explicitly addressed by the Code design curves; however, recent test data illustrate the detrimental effects of LWR coolant environments on the fatigue resistance of austenitic stainless steels (SSs). Certain loading and environmental conditions have led to test specimen fatigue lives that are significantly shorter than those obtained in air. Results of fatigue tests that examine the influence of reactor environments on crack initiation and crack growth of austenitic SSs are presented. Block loading was used to mark the fracture surface to determine crack length as a function of fatigue cycles in water environments. Crack lengths were measured by scanning electron microscopy. The mechanism for decreased fatigue life in LWR environments is discussed, and crack growth rates in the smooth fatigue specimens are compared with existing data from studies of crack growth rates.

## INTRODUCTION

The rules for the construction of Class 1 components for nuclear power plants, contained in the ASME Boiler and Pressure Vessel Code Section III, Subsection NB, recognize fatigue as a possible mode of failure in pressure vessel and piping materials. Cyclic loading occurs on a structural component because of changes in mechanical and thermal loads as the system goes from one set of pressure, temperature, moment, and force loading conditions to any other set of conditions. Figures I-9.1 through I-9.6 of Appendix I to Section III of the Code specify fatigue design curves that define the allowable number of cycles as a function of applied stress amplitude. However, Subsection NB-3121 of Section III states that the data on which the fatigue design curves are based did not address the effect of the coolant environment on the fatigue resistance of a material. Recent fatigue strain-vs.-life (S-N) data illustrate potentially significant effects of light water reactor (LWR) coolant environments on the fatigue resistance of pressure vessel and piping materials (Chopra and Shack, 1995a,1995b,1997; Higuchi and Iida, 1991,1995; Mimaki et al., 1996; Shack and Burke, 1991)

A program is being conducted at Argonne National Laboratory to provide data and models for predicting the effects of environment on fatigue design curves and to assess the validity of fatigue damage summation in piping and vessel steels under load histories typical of LWR components. Based on existing fatigue S-N data, interim fatigue design curves that address environmental effects on fatigue life of austenitic stainless steels (SSs) have been proposed (Majumdar et al., 1993). Statistical models have been developed for estimating the effects of various material and loading conditions on fatigue lives of materials used in the construction of nuclear power plant components (Keisler et al., 1995, 1996).

This paper presents the results of fatigue tests that examine the influence of the reactor environment on the formation and growth of fatigue cracks in polished smooth specimens of austenitic SSs. Fatigue tests have been conducted on Type 304 SS to determine the crack initiation and crack growth characteristics of this material in air and LWR environments. The effects of LWR environments on growth of short cracks are discussed.

## MECHANISM OF FATIGUE CRACK INITIATION

The fatigue S–N curve represents the process of fatigue crack initiation. In the existing fatigue S-N data base, fatigue life is defined as the number of cycles for tensile stress to decrease 25% from its peak value. For most fatigue test specimens, the decrease in tensile stress corresponds to a crack ≈3 mm deep; a crack of this size is referred to as an engineering crack. For a given stress or strain amplitude, the S-N curve specifies the number of cycles needed to form an engineering crack, i.e., a 3-mm-deep crack; the number of cycles required to form this crack is defined as the fatigue life of the material. Deformation and microstructural changes in the surface grains control fatigue cracking. During cyclic straining, the irreversible nature of dislocation glide leads to the development of surface roughness, and strain localization in persistent slip bands

## DISCLAIMER

## DISCLAIMER

Portions of this document may be illegible in electronic image products. Images are produced from the best available original document.

(PSBs) leads to the formation of extrusions and intrusions. With continued cycling, microcracks ultimately form in PSBs or at the edges of slip–band extrusions. At high strain amplitudes, microcracks form in notches that develop at grain or twin boundaries. Similarly, microcracks can also develop at phase boundaries, such as ferrite/pearlite boundaries, or by cracking of second–phase particles, such as sulfide or oxide inclusions.

Once a microcrack is formed, it continues as a Mode II shear crack in Stage I growth along its slip plane or along a PSB and grows at an orientation 45° to the stress axis. At low strain amplitudes, a Stage I crack may extend across several grain diameters before the increasing stress intensity of the crack promotes slip on systems other than the primary slip plane. Once slip is no longer confined to planes at 45° to the stress axis, the crack begins to propagate as a Mode I tensile crack normal to the stress axis in Stage II growth. At high strain amplitudes, the stress intensity is quite large and the crack propagates entirely by the Stage II process. The Stage II crack propagation continues until the crack reaches engineering size (3 mm). Stage II fracture in air or mildly corrosive environments is characterized by fatigue striations.

Fatigue life, or number of allowable cycles, has conventionally been represented by two stages: initiation, which represents the cycles $N_i$ that are necessary for the formation of microcracks on the surface; and propagation, which represents the cycles $N_p$ needed for propagation of the surface cracks to an engineering size. Thus, fatigue life N is the sum of the two stages, $N = N_i + N_p$. Crack initiation is considered sensitive to the stress or strain amplitude such that, at low strain amplitudes, most of the life may be spent in initiating a crack, whereas, at high strain amplitudes, cracks initiate easily.

An alternative approach to crack initiation and growth considers fatigue life to be entirely composed of crack propagation (Miller, 1995). A measure of fatigue damage in a material is the current size of a fatigue crack; damage accumulation is the rate of crack growth. During fatigue loading of smooth test specimens, cracks form immediately at surface irregularities or discontinuities that are either already in existence or are produced by slip bands, grain boundaries, second–phase particles, etc. (Fig. 1). Growth of these surface cracks may be divided into three regimes: an initial period that involves growth of microstructurally small cracks (MSCs) and is characterized by decelerating crack growth, seen in Region AB of Fig. 1; a final period of growth that is characterized by accelerating crack growth, Region CD; and a transition period that is controlled by a combination of these two regimes, Region BC.

Below a critical crack length, the growth of MCSs is very sensitive to microstructure (Tokaji et al., 1986; Tokaji and Ogawa, 1992; Tokaji et al., 1988; de los Rios et al., 1992). In the early stage of growth, the MSCs correspond to Stage I cracks and grow along slip planes as shear cracks. Microstructural effects are strong because of the crystallographic nature of Stage I growth, and the growth rates are markedly decreased by grain boundaries, triple points, and phase boundaries. Limited data suggest that microstructural effects are more pronounced at negative stress ratios; the compressive component of the applied load plays an important role in the formation of Stage I facets and in acting as a crack driving force (Tokaji and Ogawa, 1992). Above the critical length of MSCs, fatigue cracks show little or no influence of microstructure and are

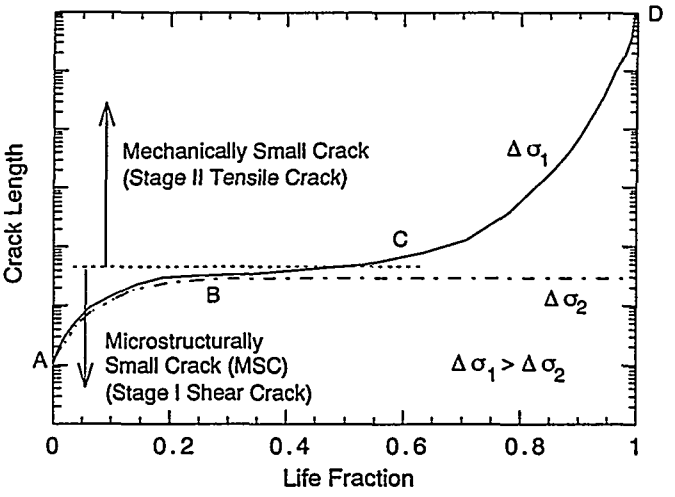


**Figure 1. Growth of cracks in smooth fatigue specimens**

termed mechanically small cracks (Tokaji and Ogawa, 1992); their growth rates are higher than those of large cracks because they exhibit less crack closure. These mechanically small cracks correspond to Stage II or tensile cracks that are characterized by striated crack growth with a fracture surface that is normal to the maximum principal stress. For a stress ratio of –1, the transition from an MSC to a mechanically small crack in several materials has been estimated to be approximately eight times the microstructural unit size (Tokaji and Ogawa, 1992).

At low stress levels ($\Delta\sigma_2$ in Fig. 1), the transition from MSC growth to accelerating crack growth does not occur and results in nonpropagating cracks. This lack of transition represents the fatigue limit for the smooth specimen. It is not a stress limit below which cracks cannot form, but a limit below which microcracks that form on smooth surfaces can not grow to engineering size. Large cracks that may preexist in the material or be created by growth of microcracks at high stresses can grow at stress levels below the fatigue limit.

The reduction in fatigue life in LWR coolant environments may arise from easier formation of surface microcracks or an increase in growth rates of cracks during either initial shear crack growth stage or final tensile crack growth. Specimens tested in water have crystalline oxides and a thin gray corrosion scale. X-ray diffraction analyses of these specimens indicate that the corrosion scale consists primarily of iron and chromium oxides such as $Fe_3O_4$, $FeFe_2O_4$, $\gamma$-$Fe_2O_3$, and CrO and in the case of high-dissolved-oxygen (DO) water, $\alpha$-$Fe_2O_3$. In addition to corrosion scales, the specimens tested in water also show some surface micropitting.

The presence of micropits, which act as stress raisers and provide preferred sites for the formation of fatigue cracks, has been thought to contribute to the reduction of fatigue life in high-temperature water. However, fatigue data for carbon and low-alloy steels indicate that the presence of micropits alone cannot explain the large reductions in fatigue lives of these steels in LWR environments (Chopra and Shack, 1988). Specimens preexposed to high-DO water and subsequently tested in air do not show a reduction in fatigue life, as would be expected if micropits were the only contributor, and

**Table 1: Composition (wt. %) of Type 304 austenitic stainless steel used for fatigue tests**

| Material | C | P | S | Si | Cr | Ni | Mn | Mo | Cu | N |
|---|---|---|---|---|---|---|---|---|---|---|
| Type 304[a] (Heat 309556) | 0.060 | 0.019 | 0.007 | 0.48 | 18.99 | 8.00 | 1.54 | 0.44 | --- | 0.100 |

[a]Solution annealed at 1050°C for 0.5 h.

specimens that have been preoxidized in low-DO water show a moderate decrease in life when compared with unoxidized specimens.

The enhanced growth rates of pressure vessel and piping materials in LWR environments have been attributed to either slip dissolution (Ford et al., 1993; Ford, 1986) or hydrogen–induced cracking (Hänninen et al., 1986) mechanisms. The slip dissolution model requires the formation of a thermodynamically stable passive oxide film to ensure that a crack will propagate with a high aspect ratio without degrading into a blunt pit. Also a strain increment must occur to rupture the oxide film thereby exposing the underlying matrix to the environment. Once the passive oxide film is ruptured, crack extension is controlled by the dissolution of freshly exposed surfaces and the re-formation kinetics of the oxide film. Hydrogen–induced cracking of steels occurs when hydrogen produced by the oxidation reaction at or near the crack tip is partly absorbed into the metal; absorbed hydrogen diffuses ahead of the crack tip and interacts with inclusions leading to the formation of cleavage cracks at the inclusion/matrix interface; and linkage of the cleavage cracks produces discontinuous crack extension in addition to that caused by mechanical fatigue. Both mechanisms depend on oxide rupture rates, passivation rates, and liquid diffusion rates; therefore, it is difficult to differentiate between the two mechanisms. The presence of well-defined fatigue striations suggests that hydrogen-induced cracking may be responsible for environmentally-assisted reduction in fatigue lives of austenitic SSs.

## EXPERIMENTAL

Low-cycle fatigue tests have been conducted on Type 304 austenitic SSs, which had been solution annealed at 1050°C for 0.5 hour. The composition of the material is given in Table 1. Smooth cylindrical specimens with 9.5-mm-diameter and 19-mm gauge length were used for the fatigue tests. Prior to testing, the specimen gauge length was given a 1-μm surface finish. The surface finish was applied in the axial direction to prevent circumferential scratches which might act as crack initiation sites.

All tests were conducted at 288°C with fully reversed axial loading (i.e., R = -1) and a triangular or sawtooth waveform. The strain rate for the triangular wave and the fast-loading half of the sawtooth wave was 0.4%/s. The tests in air were performed under strain control with an axial extensometer, and specimen strain was measured at two points outside the gauge region. The data that were obtained were then used to determine the stroke required to maintain a constant strain in the specimen gauge section for tests in water environments. Tests in water were conducted in a small autoclave under stroke control where the specimen strain was controlled between two locations outside the autoclave. The feed water for the low-DO simulated pressurized water reactor (PWR) environment contained <0.01 ppm DO, 2 ppm lithium, 1000 ppm boron, and ≈2 ppm dissolved hydrogen (≈23 cc/kg), and it had a pH of ≈6.5 and a conductivity of ≈19.2 μS/cm. The feed water for the high-DO simulated boiling water reactor (BWR) environment contained ≈0.7 ppm DO and had a pH of ≈6.0 and a conductivity of ≈0.09 μS/cm. The chemical analyses of the feed water were conducted at room temperature. The fatigue tests were performed using both a once-through and a recirculating water system. Details of the test facility and procedure are described in Chopra and Shack (1995a).

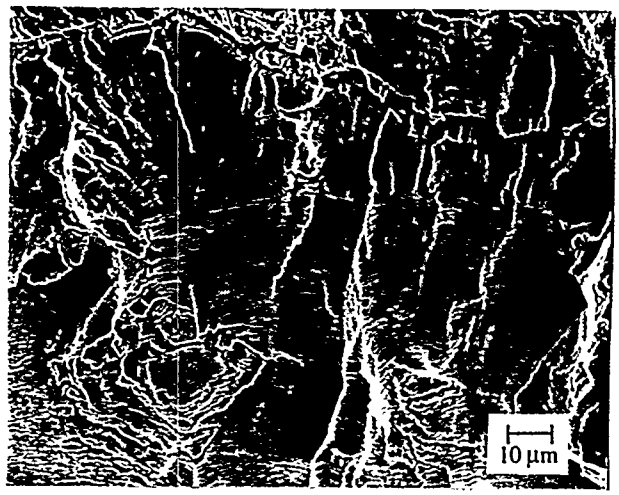


**Figure 2. Photomicrograph showing the difference in striation spacing formed by the fast/fast (top of photo) and slow/fast (bottom of photo) blocks of cycles**

Crack growth characteristics for the high-temperature water tests were determined by block loading. The slow/fast sawtooth loading was interrupted at approximately 500 cycle intervals, and the specimen was subjected to a block of triangular fast/fast loading cycles at a lower strain range. This method has been used successfully to characterize crack growth in A333-Gr 6 carbon steel tested in 288°C water with ≈0.8 ppm DO (Higuchi et al., 1997). In tests using carbon and low-alloy steels, the block of fast/fast cycles leaves distinct beach marks on the fracture surface that can be used to characterize crack size as a function of fatigue cycles for the slow/fast test. In stainless steels, the beach marks are less prominent, and extensive microscopy is required to reveal the features on the fracture surface associated with the loading blocks.

After an initial microscopic examination, the oxide film was removed from the fracture surface by soaking the specimen in a hot solution of potassium permanganate (80 vol.%) and sodium hydroxide (20 vol.%) for one hour, rinsing in distilled water, soaking for an additional hour in a hot solution of ammonium citrate (20 vol.%) and water, and finally rinsing in an ultrasonic bath of acetone. Once the fracture surface was cleaned, the regions of fast/fast loading blocks could be readily distinguished, as seen in Fig. 2. The regions of fast/fast blocks were then mapped onto a large composite photomicrograph of the fracture surface. Assuming that each striation corresponded to one cycle, the number of striations between the last observed fast/fast block and the onset of ductile (tensile) failure were counted to verify the location of the last block. The remaining visible fast/fast blocks were numbered sequentially toward the initiation site. Figure 3 shows schematic representations of the fracture surfaces and the probable crack fronts as determined by electron microscopy.

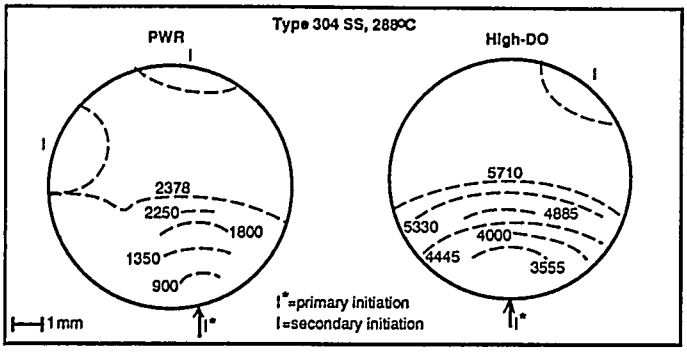


**Figure 3. Fracture surface and probable crack front (dashed lines) after different fast/fast loading cycles for PWR and high-DO water environments**

## RESULTS

### Fatigue Life

The fatigue S-N data for Type 304 SS in air and water at 288°C are given in Table 2; the results are plotted in Fig. 4. The ASME mean data curve and the best-fit curves in air, simulated PWR, and high-DO water based on the statistical model (Chopra and Smith, 1998) are also shown in Fig. 4. For convenience, the statistical model correlations are given below. For a strain rate of 0.004%/s, the fatigue life N for Type 304 SS in air at 288°C is

$$\ln(N) = 6.196 - 2.030\ln(\varepsilon_a - 0.126) \quad (1)$$

where $\varepsilon_a$ is the strain amplitude (%). In LWR environments, the fatigue of Type 304 SS is expressed as

$$\ln(N) = 5.768 - 2.030\ln(\varepsilon_a - 0.126) + T^*\dot{\varepsilon}^*O^* \quad (2)$$

where the constants for transformed temperature (T*), strain rate ($\dot{\varepsilon}^*$), and dissolved oxygen (O*) are defined as follows

$$\begin{aligned} T^* &= 0 && (T<200°C) \\ T^* &= 1 && (T\geq 200°C) \end{aligned} \quad (3a)$$

$$\begin{aligned} \dot{\varepsilon}^* &= 0 && (\dot{\varepsilon} > 0.4\%/s) \\ \dot{\varepsilon}^* &= \ln(\dot{\varepsilon}/0.4) && (0.4 \geq \dot{\varepsilon} \geq 0.0004\%/s) \\ \dot{\varepsilon}^* &= \ln(0.0004/0.4) && (\dot{\varepsilon} < 0.0004\%/s) \end{aligned} \quad (3b)$$

$$\begin{aligned} O^* &= 0.260 && (DO<0.05 \text{ ppm}) \\ O^* &= 0.172 && (DO\geq 0.05 \text{ ppm}) \end{aligned} \quad (3c)$$

The results indicate a significant decrease in fatigue life in water when compared with fatigue life obtained in air; the reduction in life depends both on strain rate and the dissolved oxygen content of the water. Fatigue life decreases with decreasing strain rate, and the effect is greater in a low-DO PWR environment than in a high-DO environment.

Photomicrographs of the fracture surface of Type 304 SS specimens tested with block loading in water environments are shown in Fig. 5. Both fracture surfaces consist of several cracks that were initiated at different axial and circumferential locations and did not merge into a single primary crack. The fracture surface of specimens tested at constant strain range typically consist of a single crack or a few cracks that merge to form the final fracture surface.

**Table 2. Fatigue results for Type 304 SS in air and water environments**

| Test No. | Environ. | Strain Range (%) | Strain Rate (%/s) Tensile | Strain Rate (%/s) Comp. | Stress Range (MPa) | Life $N_{25}$ (Cycles) |
|---|---|---|---|---|---|---|
| 1801 | air | 0.76 | 0.400 | 0.40 | 419.2 | 24,500 |
| 1804 | air | 0.50 | 0.400 | 0.40 | 382.8 | 61,680 |
| 1825 | air | 0.30 | 0.040 | 0.40 | 394.4 | 957,160 |
| 1805 | air | 0.76 | 0.004 | 0.40 | 467.9 | 14,410 |
| 1817 | air | 0.50 | 0.004 | 0.40 | 421.7 | 42,180 |
| 1807 | PWR | 0.51 | 0.400 | 0.40 | 374.6 | 25,900 |
| 1806 | PWR | 0.73 | 0.400 | 0.40 | 428.9 | 11,500 |
| 1810 | PWR | 0.77 | 0.040 | 0.40 | 447.6 | 5,800 |
| 1826 | PWR | 0.29 | 0.010 | 0.40 | 375.8 | 131,100 |
| 1821 | PWR | 0.76 | 0.004 | 0.40 | 474.3 | 2,420 |
| 1808 | PWR | 0.77 | 0.004 | 0.40 | 468.3 | 2,850 |
| 1823 | PWR | 0.51 | 0.004 | 0.40 | 408.2 | 6,900 |
| 1824[a] | PWR | 0.75 | 0.004 | 0.40 | 488.5 | 2,270 |
| 1827 | High-DO | 0.75 | 0.004 | 0.40 | 475.8 | 3,650 |
| 1841[b] | High-DO | 0.75 | 0.004 | 0.40 | 483.3 | 5,657 |

[a]Every 450 cycles block loaded 500 or 1000 fast/fast cycles at 0.5% strain range and 0.4%/s strain rate
[b]Every 445 cycles block loaded 700 fast/fast cycles at 0.5% strain range and 0.4%/s strain rate

### Fatigue Crack Depth

The depth of the largest crack obtained for the block loading tests in water at 288°C and ≈0.75% strain range is plotted as a function of fatigue cycles in Fig. 6 and as a function of fraction of life in Fig. 7. The data in these figures for Type 316L SS tested in air at 25°C and ≈0.006-0.02% plastic strain range (which corresponds to ≈0.3-0.32 total strain range) are from Orbtlik et al. (1997). The curve for the uninterrupted test in air at 0.75% strain range and 0.004/0.4%/s tensile/compressive strain rate (shown as a dash-dot line in Fig. 6) was calculated from the best-fit equation of the experimental data for Type 316L SS (Orbtlik et al., 1997). Studies on carbon and low-alloy steels (Tokaji et al., 1988; Dowling, 1977; Suh et al., 1985) indicate that the fatigue crack size at different life fractions is independent of strain range and strain rate; consequently, the depth of the largest crack at different life fractions is approximately the same at 0.75 and 0.3% strain ranges. The results from this study show that after 1500 cycles the crack lengths in air, high-DO water, and PWR water are ≈40, 300, and 1200 μm, respectively. At the same fraction of life, the crack lengths are longer in water than in air. Furthermore, the crack length in PWR water is greater than in high-DO water.

### Crack Growth Rate

The crack growth rates determined from the crack-depth-vs.-cycles data of Fig. 6 are plotted as a function of crack depth in Fig. 8. The crack growth rates in air are less than those in high-DO water by a factor of two and less than those in low-DO PWR water by a factor of four. The average crack growth rate at a depth of 1000 μm is 0.28, 0.70, and 1.1 μm/cycle in air, high-DO water, and PWR water,

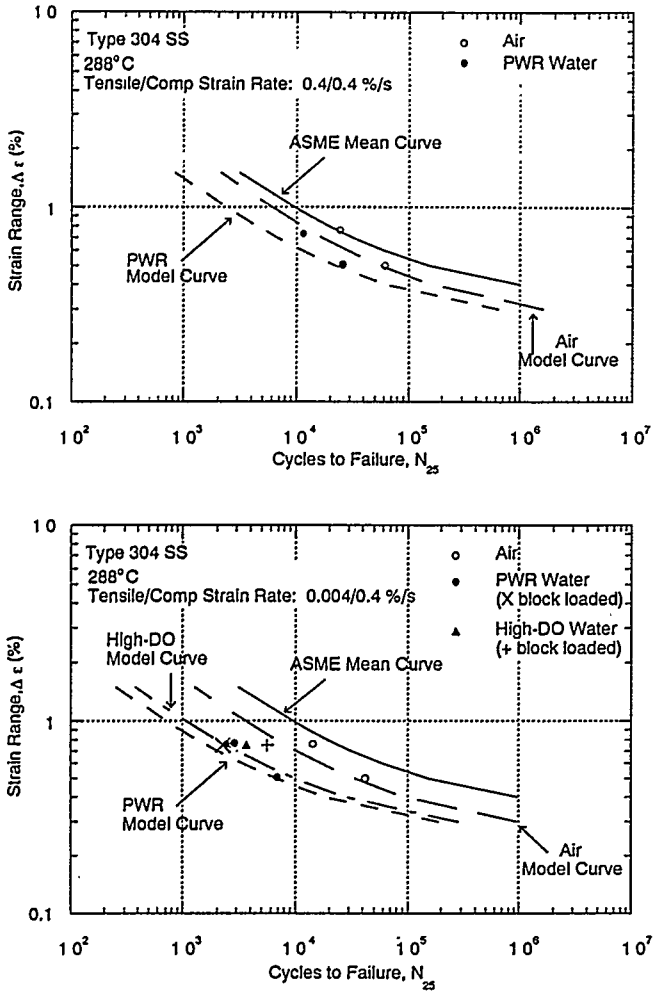


**Figure 4. Total strain range vs. fatigue life data for Type 304 SS in air and water environments at 288°C**

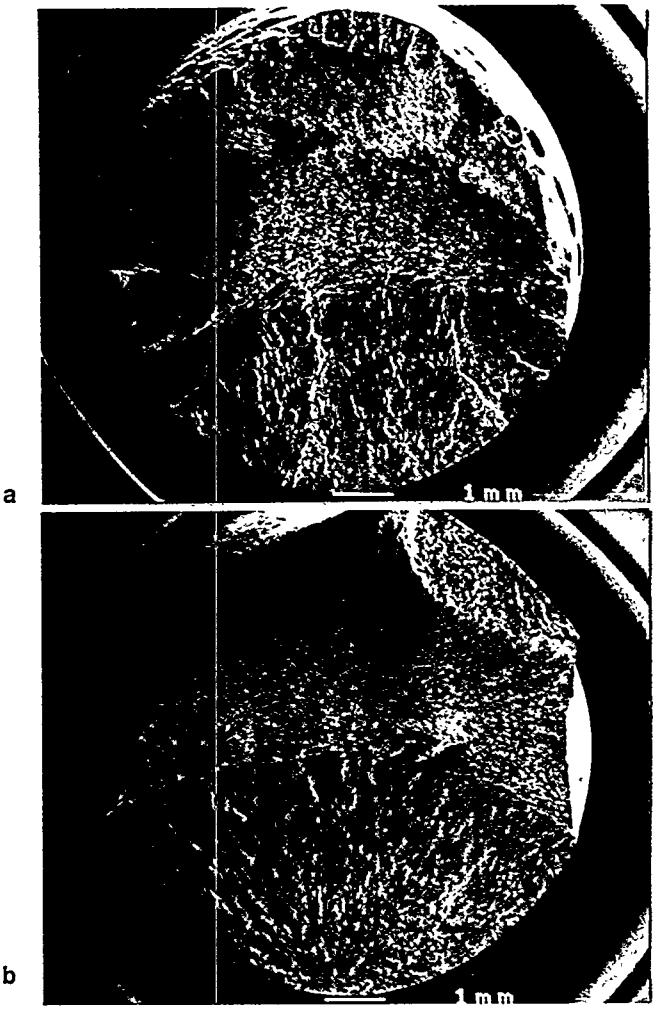


**Figure 5. Photomicrographs of fractured specimens tested with slow/fast waveforms in (a) PWR water with fast/fast blocks every 450 cycles and (b) high-DO water with fast/fast blocks every 500 cycles**

respectively. The measured crack growth rates are compared with the current ASME Section XI reference crack growth curve for austenitic SSs in Fig. 9. For cylindrical fatigue specimens, the stress intensity ranges $\Delta K$ were determined from the values of $\Delta J$, which for a small half-circular surface crack (Dowling, 1977) are given by

$$J = 3.2\left(\frac{\sigma^2}{2E}\right)a + 5.0\left(\frac{\sigma\varepsilon_p}{1+n}\right)a \qquad (4)$$

where E is the elastic modulus, $\varepsilon_p$ is the nominal plastic strain, and a is the crack depth. The stress intensities associated with conventional cylindrical fatigue specimens were modified on the basis of rigorous finite-element models (O'Donnell and O'Donnell, 1995). The cyclic stress $\sigma$ and strain $\varepsilon$ are defined as

$$\varepsilon = \frac{\sigma}{E} + \left(\frac{\sigma}{A}\right)^n \qquad (5)$$

where the constant A and the exponent n were determined from the experimental data (Chopra and Gavenda, 1998). The growth rates in air, shown by the dashed line, were determined from the estimated crack depth-vs.-fatigue life data in air, shown as the dashed curve in Fig. 6.

The results show fair agreement with the ASME Code curve for long cracks. The estimated growth rates in air are higher than those predicted by the Code curve. Fatigue tests are in progress to determine the crack initiation and growth characteristics of austenitic stainless steels in air. The growth rates in PWR water are marginally higher than those in high-DO water; although, the fatigue life is a factor of ~2 lower in PWR water. These findings indicate that the decrease in fatigue life in LWR environments is primarily due to the effect of environment during the early stages of crack initiation, i.e., the growth of cracks <500 mm deep. The increases in crack growth associated with the environment are not consistent with current models, which would generally predict higher environmental crack growth rates in high-DO environments than in PWR environments (Shack and Kassner, 1994; Gilman et al., 1988).

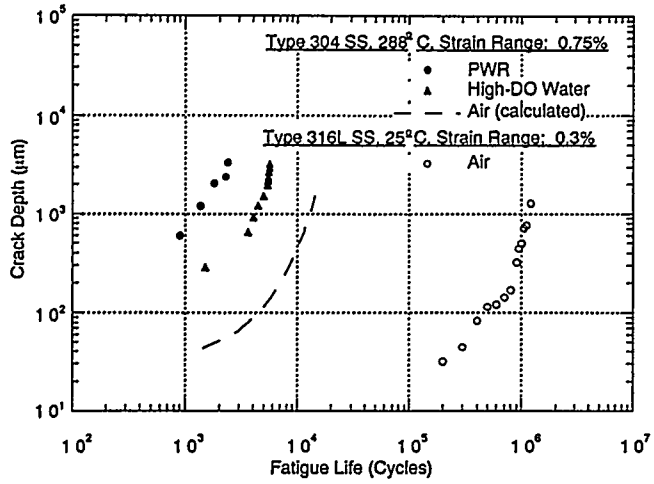


**Figure 6. Depth of largest crack plotted as a function of fatigue cycles for austenitic SSs in air and water environments. Data for Type 316L SS taken from Orbtlik et al (1997).**

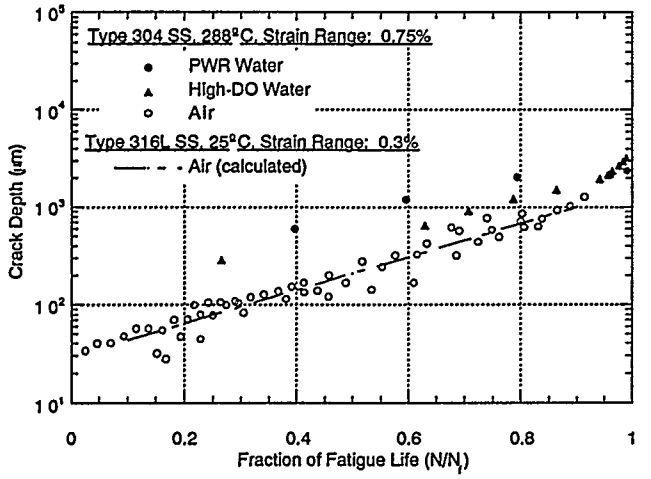


**Figure 7. Depth of largest crack plotted as a function of fraction of life for austenitic SSs in air and water environments. Data for Type 316L SS taken from Orbtlik et al (1997).**

## DISCUSSION

The results from the present study indicate that the decrease in fatigue life of austenitic stainless steels in LWR environments is primarily caused by the effects of the environment on the growth of short cracks. The number of cycles required to produce 500-μm crack is 300, 8000, and 10,000 for PWR, high-DO, and air, respectively. Relative to air, crack growth rates in low-DO water are more than one order of magnitude higher during the initial stages of fatigue damage (crack sizes of <500 μm). Metallographic examination of austenitic SS test specimens indicate that in PWR water surface cracks grow entirely as tensile cracks normal to the stress axis (Fig. 10a). In air and high-DO water, surface cracks initially grow as shear cracks oriented approximately 45° to the stress axis and then as tensile cracks

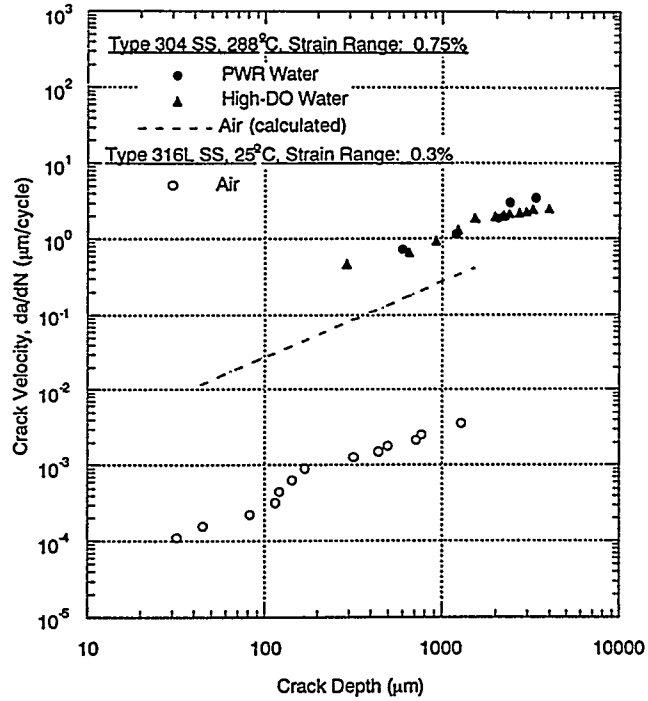


**Figure 8. Crack growth rates, determined from data in Figure 6, plotted as a function of crack depth for austenitic SSs in air and water environments**

normal to the stress axis when slip is no longer confined to shear slip planes (Fig. 10b).

For austenitic stainless steels, it is difficult to reconcile lower fatigue lives in PWR water than in high-DO water in terms of the slip dissolution mechanism despite the absence of Stage I crack growth in low-DO water. Further contradicting the slip dissolution model is the presence of well-defined striations, which are more indicative of hydrogen-induced cracking. It is possible that dissolved oxygen has an effect on one of the key elements of corrosion resistance, specifically, the passive oxide film. If dissolved oxygen affects the tenacity of the oxide film, the lower fatigue lives may be attributed to a lower rupture strain for surface oxides in low-DO water than in high-DO water. Work is currently underway to investigate the role of oxide rupture strain in crack growth.

## CONCLUSIONS

Fatigue tests have been conducted to determine the crack initiation and crack growth characteristics of austenitic stainless steels in air and LWR environments. Results of fatigue tests that examine the influence of reactor environment on the formation and growth of short cracks in Types 304 SS are presented. Crack lengths as a function of fatigue cycles were determined in air and water environments. The significant conclusions are summarized below.

- At the same fraction of life, the crack lengths are longer in water than in air. The crack growth rates in water are greater than those in air, and the crack growth rates in PWR water are greater than those in high-DO water.

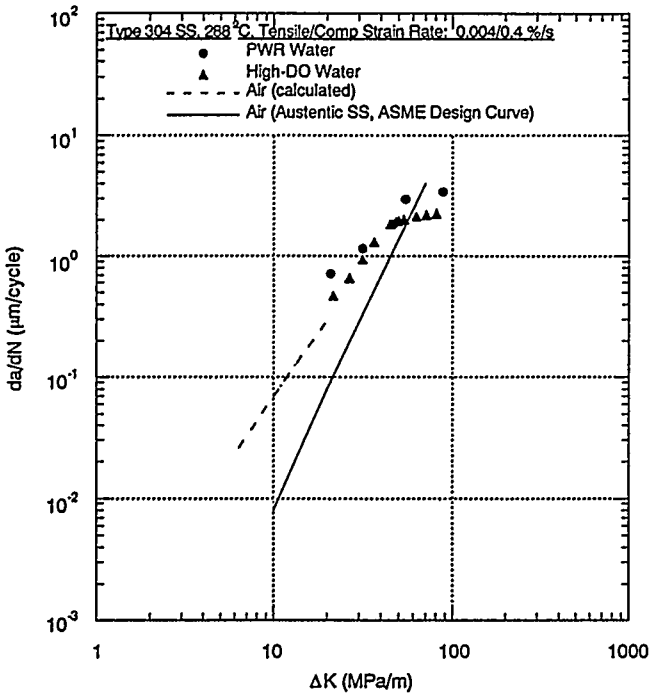


**Figure 9. Crack growth rates, determined from smooth cylindrical fatigue test specimens, and ASME Section XI reference curves for austenitic SSs in air and water environments**

- The decrease in fatigue life of Type 304 austenitic stainless steel in LWR water is primarily caused by the effects of environment on the growth of short cracks that are <500 μm deep.
- The results from the present study are not consistent with the slip dissolution model for enhanced crack growth rates in LWR environments. Oxide film rupture strengths and/or hydrogen evolution may play a greater role in these environments.

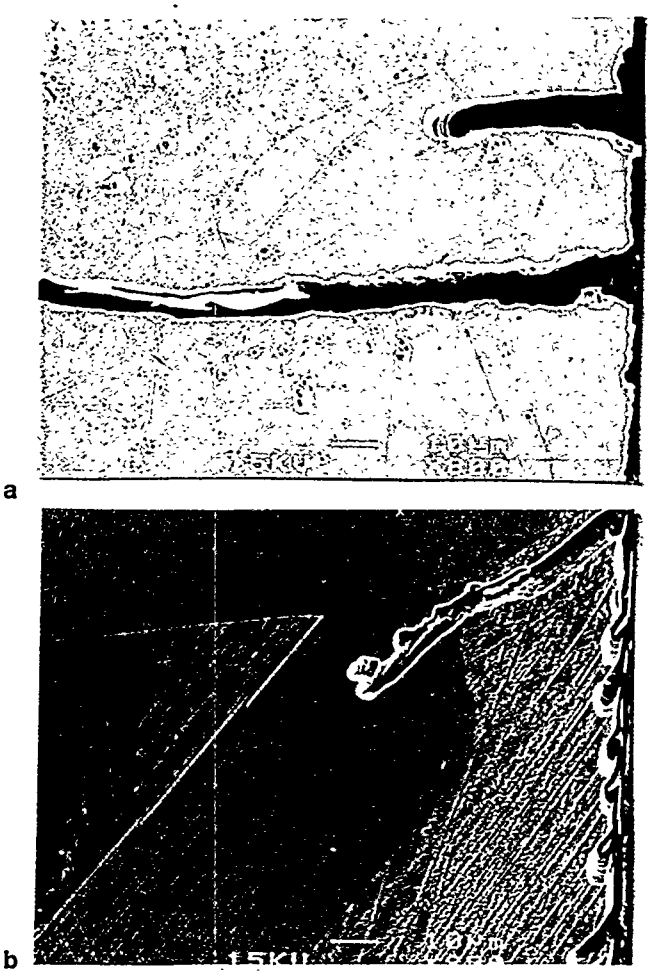


**Figure 10. Photomicrographs of surface cracks along longitudinal sections of Type 316 NG SS specimens tested at 288°C in (a) PWR and (b) high-DO water environments**


## ACKNOWLEDGMENTS

The authors thank W. F. Burke, T. M. Galvin, and J. C. Tezack for their contributions to the experimental effort. This work was sponsored by the Office of Nuclear Regulatory Research, U.S. Nuclear Regulatory Commission. FIN Number W6610; Program Manager: Dr. M. McNeil.


## REFERENCES


Chopra, O. K., and Gavenda, D. J., 1998, "Effects of LWR Coolant Environments on Fatigue Lives of Austenitic Stainless Steels," *Trans. of ASME*, **120**, pp. 116-121.

Chopra, O. K., and Shack, W. J., 1995a, "Effects of LWR Environments on Fatigue Life of Carbon and Low–Alloy Steels," in *Fatigue and Crack Growth: Environmental Effects, Modeling Studies, and Design Considerations*, PVP Vol. 306, S. Yukawa, ed., American Society of Mechanical Engineers, New York, pp. 95–109.

Chopra, O. K., and Shack, W. J., 1995b, "Effects of Material and Loading Variables on Fatigue Life of Carbon and Low–Alloy Steels in LWR Environments," in *Transactions of 13th Int. Conf. on Structural Mechanics in Reactor Technology (SMiRT 13)*, Vol. II, M. M. Rocha and J. D. Riera, eds., Escola de Engenharia – Universidade Federal do Rio Grande do Sul, Porto Alegre, Brazil, pp. 551–562.

Chopra, O. K., and Shack, W. J., 1997, "Evaluation of Effects of LWR Coolant Environments on Fatigue Life of Carbon and Low–Alloy Steels," to be published in *Proc. of Symposium on Effects of the Environment on the Initiation of Crack Growth*, ASTM STP 1298, American Society for Testing and Materials, Philadelphia.

Chopra, O. K., and Shack, W. J., 1997, "Evaluation of Effects of LWR Coolant Environments on Fatigue Life of Carbon and Low-Alloy Steels," *Proc. of Symposium on Effects of the Environment on the Initiation of Crack Growth*, ASTM STP 1298, W. A. Van Der Sluys, R. S. Piascik, and R. Zawierucha, eds., American Society for Testing and Materials, Philadelphia, pp. 247-266.

Chopra, O. K., and Shack, W. J., 1998 "Effects of LWR Coolant Environments on Fatigue Design Curves of Carbon and Low-Alloy Steels," NUREG/CR-6583, ANL-97/18.

Chopra, O. K., and Smith, J. L., 1998, "Estimation of Fatigue Strain-Life Curves for Austenitic Stainless Steels in Light Water Reactor Environments," in *Fatigue, Environmental Factors, and New Materials*, PVP Vol. 374, H. S. Mehta et al, eds., American Society of Mechanical Engineers, New York, pp. 249-259.

de los Rios, E. R., Navarro, A., and Hussain, K., 1992, "Microstructural Variations in Short Fatigue Crack Propagation of a C–Mn Steel," in *Short Fatigue Cracks*, ESIS 13, M. J. Miller and E. R. de los Rios, eds., Mechanical Engineering Publication, London, pp. 115–132.

Dowling, N. E., 1977, "Crack Growth During Low–Cycle Fatigue of Smooth Axial Specimens," in Cyclic Stress–Strain and Plastic Deformation Aspects of Fatigue Crack Growth, ASTM STP 637, American Society for Testing and Materials, Philadelphia, PA, pp. 97–121.

Ford, F. P., 1986, "Overview of Collaborative Research into the Mechanisms of Environmentally Controlled Cracking in the Low Alloy Pressure Vessel Steel/Water System," in *Proc. 2nd Int. Atomic Energy Agency Specialists' Meeting on Subcritical Crack Growth*, NUREG/CP–0067, MEA–2090, Vol. 2, pp. 3–71.

Ford, F. P., Ranganath, S., and Weinstein, D., 1993, "Environmentally Assisted Fatigue Crack Initiation in Low–Alloy Steels – A Review of the Literature and the ASME Code Design Requirements," EPRI Report TR–102765.

Gilman, J. D., Rungta, R., Hinds, P., and Mindlan, H., 1988. "Corrosion-Fatigue Crack Growth Rates in Austenitic Stainless Steels in Light Water Reactor Environments," Int. J. Pressure Vessel Piping **31**, pp. 55-68.

Hänninen, H., Törrönen, K., and Cullen, W. H., 1986, "Comparison of Proposed Cyclic Crack Growth Mechanisms of Low Alloy Steels in LWR Environments," in *Proc. 2nd Int. Atomic Energy Agency Specialists' Meeting on Subcritical Crack Growth*, NUREG/CP–0067, MEA–2090, Vol. 2, pp. 73–97.

Higuchi, M., and Iida, K., 1991, "Fatigue Strength Correction Factors for Carbon and Low–Alloy Steels in Oxygen–Containing High–Temperature Water," *Nucl. Eng. Des.* **129**, pp. 293–306.

Higuchi, M., Iida, K., and Asada, Y., 1995, "Effects of Strain Rate Change on Fatigue Life of Carbon Steel in High–Temperature Water," in *Fatigue and Crack Growth: Environmental Effects, Modeling Studies, and Design Considerations*, PVP Vol. 306, S. Yukawa, ed., American Society of Mechanical Engineers, New York, pp. 111–116.

Higuchi, M., Iida, K., and Asada, Y., 1997, "Effects of Strain Rate Change on Fatigue Life of Carbon Steel in High–Temperature Water," in Fatigue and Crack Growth: Environmental Effects, Modeling Studies, and Design Considerations, PVP Vol. 306, S. Yukawa, ed., American Society of Mechanical Engineers, New York, pp. 111-116, 1995; also in *Proc. of Symposium on Effects of the Environment on the Initiation of Crack Growth*, ASTM STP 1298, American Society for Testing and Materials, Philadelphia.

Keisler, J., Chopra, O. K., and Shack, W. J., 1995, "Fatigue Strain–Life Behavior of Carbon and Low–Alloy Steels, Austenitic Stainless Steels, and Alloy 600 in LWR Environments," NUREG/CR–6335, ANL–95/15.

Keisler, J., Chopra, O. K., and Shack, W. J., 1996, "Fatigue Strain–Life Behavior of Carbon and Low–Alloy Steels, Austenitic Stainless Steels, and Alloy 600 in LWR Environments," *Nucl. Eng. Des.* **167**, pp. 129-154.

Majumdar, S., Chopra, O. K., and Shack, W. J., 1993, "Interim Fatigue Design Curves for Carbon, Low–Alloy, and Austenitic Stainless Steels in LWR Environments," NUREG/CR–5999, ANL–93/3.

Miller, K. J., 1995, "Damage in Fatigue: A New Outlook," in *International; Pressure Vessels and Piping Codes and Standard: Volume 1 – Current Applications*, PVP Vol. 313–1, K. R. Rao and Y. Asada, eds., American Society of Mechanical Engineers, New York, pp. 191–192.

Mimaki, H., Kanasaki, H., Suzuki, I., Koyama, M., Akiyama, M., Okubo, T., and Mishima, Y., 1996, "Material Aging Research Program for PWR Plants," *Aging Management Through Maintenance Management,* ASME PVP-Vol. 332, I. T. Kisisel, ed., American Society Of Mechanical Engineers, New York, pp. 97-105.

O'Donnell, T. P., and O'Donnell, W. J., 1995, "Stress Intensity Values in Conventional S–N Fatigue Specimens," in Fatigue and Crack Growth: International Pressure Vessels and Piping Codes and Standards: Volume 1 – Current Applications, PVP Vol. 313–1, K. R. Rao and Y. Asada, eds., American Society of Mechanical Engineers, New York, pp. 195–197.

Orbtlík, K., Polák, J., Hájek, M., and Vasek, A., 1997, "Short Fatigue Crack Behaviour in 316L Stainless Steel," *Int. J. Fatigue* **19**, pp. 471-475.

Shack, W. J., and Burke, W. F., 1991, "Fatigue of Type 316NG SS," *Environmentally Assisted Cracking in Light Water Reactors,* Semiannual Report, October 1989-March 1990, NUREG/CR-4667 Vol. 10, ANL-91/5, pp. 3-19.

Shack, W. J., and Kassner, T. F., 1994, "Review of Environmental Effects on Fatigue Crack Growth of Austenitic Stainless Steels," NUREG/CR-6176, ANL-94/1.

Suh, C. M., Yuuki, R., and Kitagawa, H., 1985, "Fatigue Microcracks in a Low Carbon Steel," *Fatigue Fract. Engng. Mater. Struct.* **8**, pp. 193-203.

Tokaji, K., Ogawa, T., and Harada, Y., 1986, "The Growth of Small Fatigue Cracks in a Low Carbon Steel; The Effect of Microstructure and Limitations of Linear Elastic Fracture Mechanics," *Fatigue Fract. Engng. Mater. Struct.* **9**, pp. 205–217.

Tokaji, K., Ogawa, T., and Osako, S., 1988, "The Growth of Microstructurally Small Fatigue Cracks in a Ferritic–Pearlitic Steel," *Fatigue Fract. Engng. Mater. Struct.* **11**, pp. 331–342.

Tokaji, K., and Ogawa, T., 1992, "The Growth of Microstructurally Small Fatigue Cracks in Metals," in *Short Fatigue Cracks*, ESIS 13, M. J. Miller and E. R. de los Rios, eds., Mechanical Engineering Publication, London, pp. 85–99.